Syndecan-4 tunes cell mechanics by activating the kindlin-integrin-RhoA pathway

Antonios Chronopoulos[1†], Stephen D. Thorpe[2†*], Ernesto Cortes[1], Dariusz Lachowski[1], Alistair J. Rice[1], Vasyl V. Mykuliak[3,4], Tomasz Róg[5], David A. Lee[2], Vesa P. Hytönen[3,4*], Armando E. del Río Hernández[1*]

[1]Cellular and Molecular Biomechanics Laboratory, Department of Bioengineering, Imperial College London, London, United Kingdom

[2]Institute of Bioengineering, School of Engineering and Materials Science, Queen Mary University of London, London, United Kingdom

[3]Faculty of Medicine and Health Technology and BioMediTech, Tampere University, Tampere, Finland

[4]Fimlab Laboratories, Tampere, Finland

[5]Department of Physics, University of Helsinki, Helsinki, Finland

[†]These authors contributed equally: Antonios Chronopoulos, Stephen D. Thorpe.

*Correspondence should be addressed to A.E.d.R.H. (a.del-rio-hernandez@imperial.ac.uk), V.P.H. (vesa.hytonen@tuni.fi) or S.D.T. (s.thorpe@qmul.ac.uk).

Supplementary Information

- Supplementary Figures
- Supplementary Discussion
- Supplementary Methods
- Supplementary References

Supplementary Figures

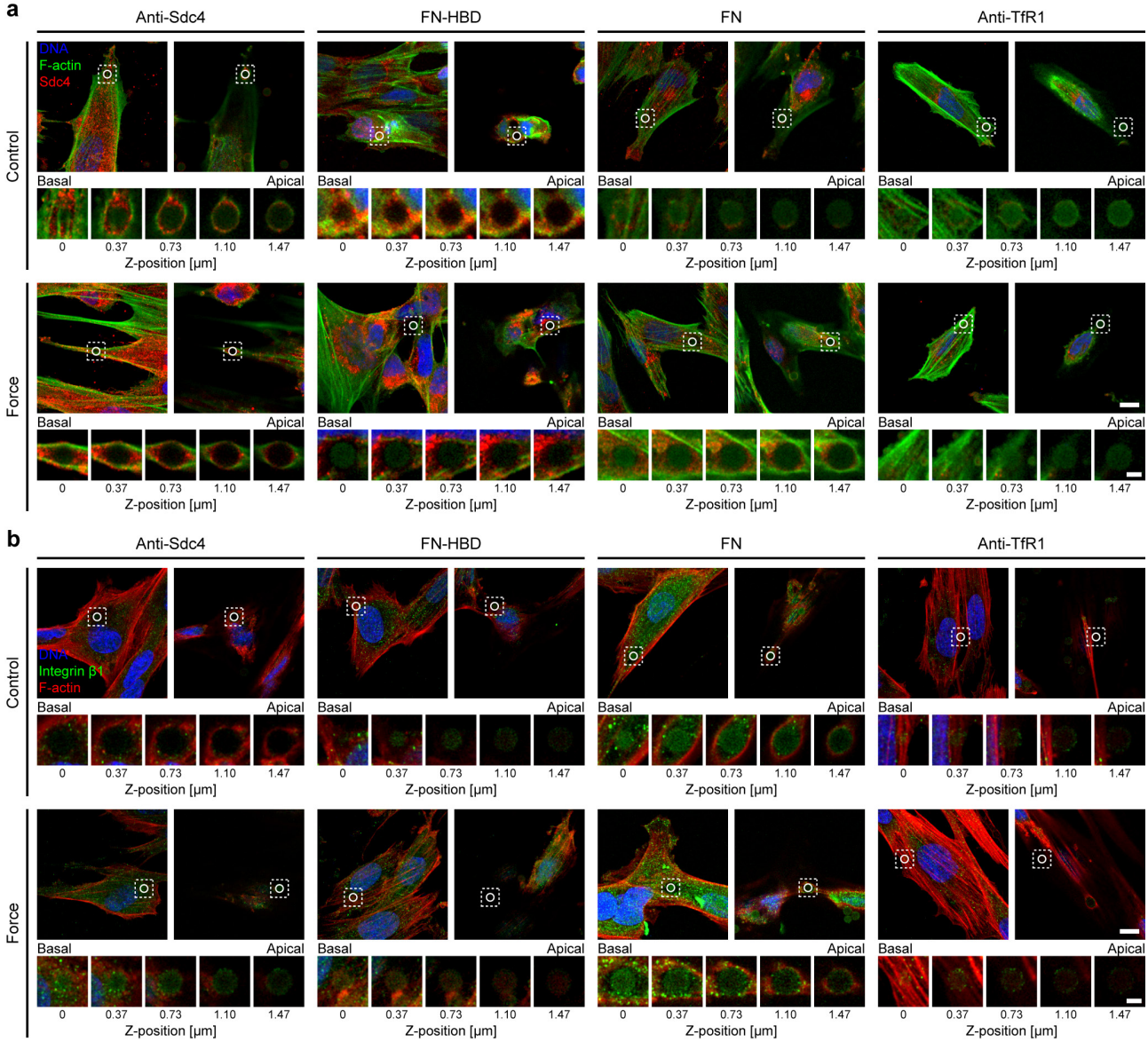

Supplementary Figure 1: Specificity of functionalised bead binding to syndecan-4. a,b, Immunofluorescent staining for (**a**) syndecan-4 (Sdc4) and (**b**) integrin β1 with f-actin and DNA as indicated. Representative basal and apical confocal z-sections are presented with higher magnification insets of the bead attachment region at a z-section spacing of 0.366 µm. To assess the specificity of cell binding to functionalised beads, pancreatic stellate cells were plated on fibronectin coated coverslips and beads allowed to attach for 30 min. Beads were functionalised with mouse anti-syndecan-4 (Anti-Sdc4) ectodomain antibody, the heparin binding domain fragment of fibronectin (FN-HBD), unmodified fibronectin (FN), and mouse anti-transferrin receptor protein-1 (Anti-TfR1). Unbound beads were removed with a PBS wash. A permanent magnet was used to apply a sustained force of approx. 200 pN to cell-bound beads for 5 min. Cells were fixed immediately post force application, and immunofluorescently stained followed by confocal imaging of bead attachment sites. Note the presence of intense syndecan-4 (red) staining in the bead attachment region in beads functionalised with anti-Sdc4, FN-HBD and FN, and the absence of this in anti-TfR1 beads in (**a**). Similarly note the absence of integrin β1 (green) surrounding beads in control (unstimulated) anti-Sdc4, FN-HBD and Anti-TfR1 beads in (**b**). Force led to accumulation of Sdc4 and/or integrin β1 at the bead site for anti-Sdc4, FN-HBD and FN beads, while no increase was evident for anti-TfR1 beads which do not elicit a mechanoresponse. Experiments were repeated independently twice with consistent results. Full field scale bar 10 µm; inset scale bar 2.5 µm.

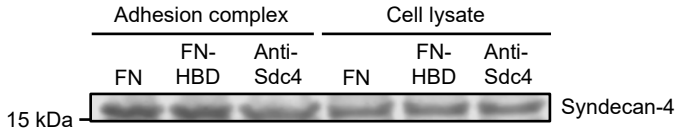

Supplementary Figure 2: Western blot confirming syndecan-4 (Sdc4) binding to functionalised cell-bound beads. Syndecan-4 is present in the adhesion complex with fibronectin (FN), 40K Heparin binding domain of fibronectin (FN-HBD), and anti-syndecan-4 antibody (Anti-Sdc4) coated beads. Functionalised beads were allowed attach to pancreatic stellate cells for 30 min before cell lysis and magnetic isolation of the bead bound adhesion complex. Representative blot from three independent experiments with similar results.

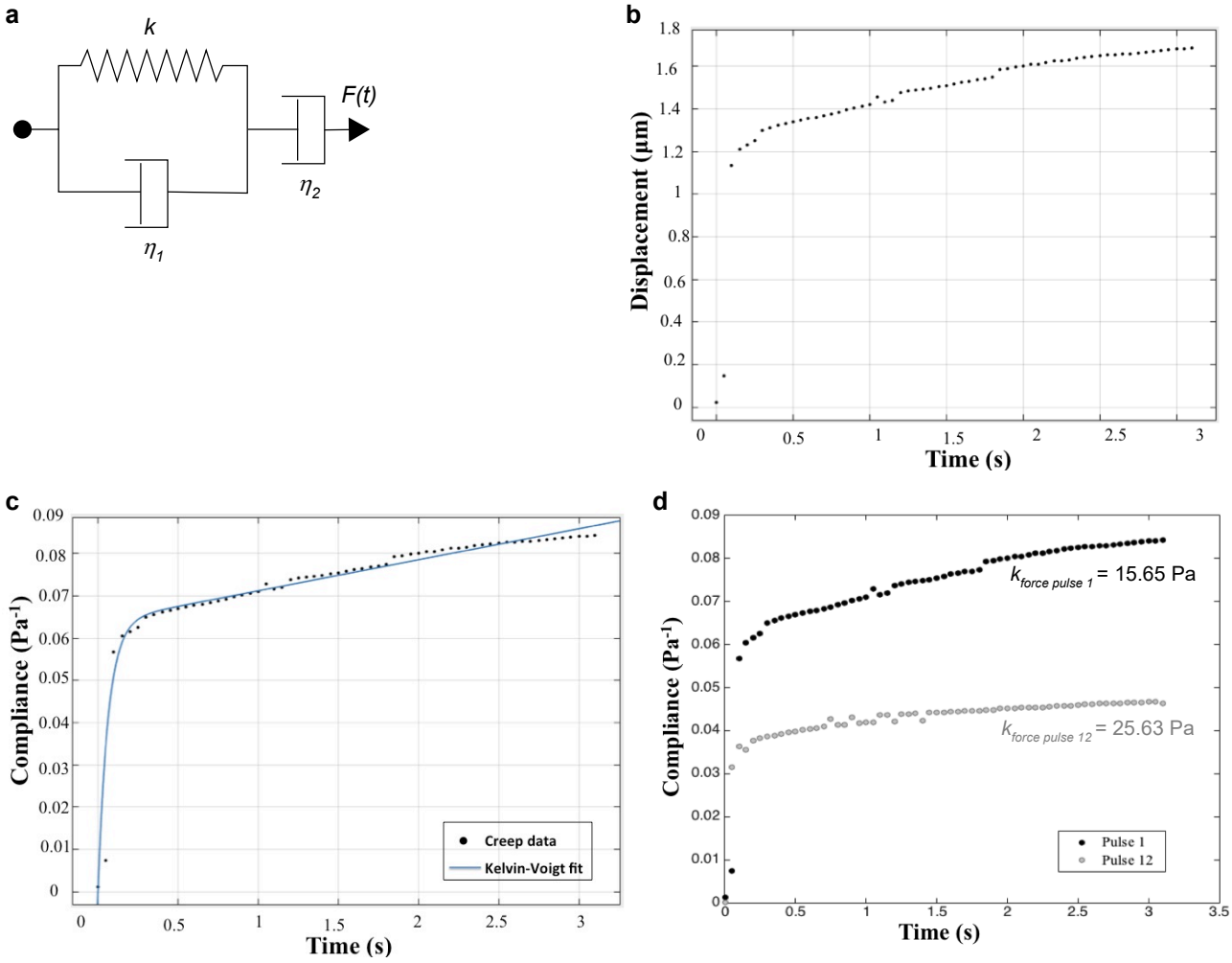

Supplementary Figure 3: Tension on syndecan-4 increases cellular stiffness. To examine the cell stiffness in response to an applied force, the time-dependent compliance ($J(t)$) of the cell was calculated from the time-dependent bead displacement ($x(t)$) using $J(t)=6\pi ax(t)/F(t)$, where a is the bead radius. The viscoelastic response of the cell was characterized by fitting the creep compliance during force application to a modified Kelvin-Voigt model used to describe viscoelastic materials. **a,** Schematic representation of the modified Kelvin-Voigt model comprising a spring and dashpot in parallel, with a dashpot in series. **b,** Representative bead displacement curve for first force pulse. **c,** Representative bead displacement curve transformed into compliance and fitted to the modified Kelvin-Voigt model. **d,** Comparison of cell stiffness denoted by the spring constant k during the first and last 1 nN force pulse. Representative cell stiffness matches data presented in Figure 1b from n = 32 cells.

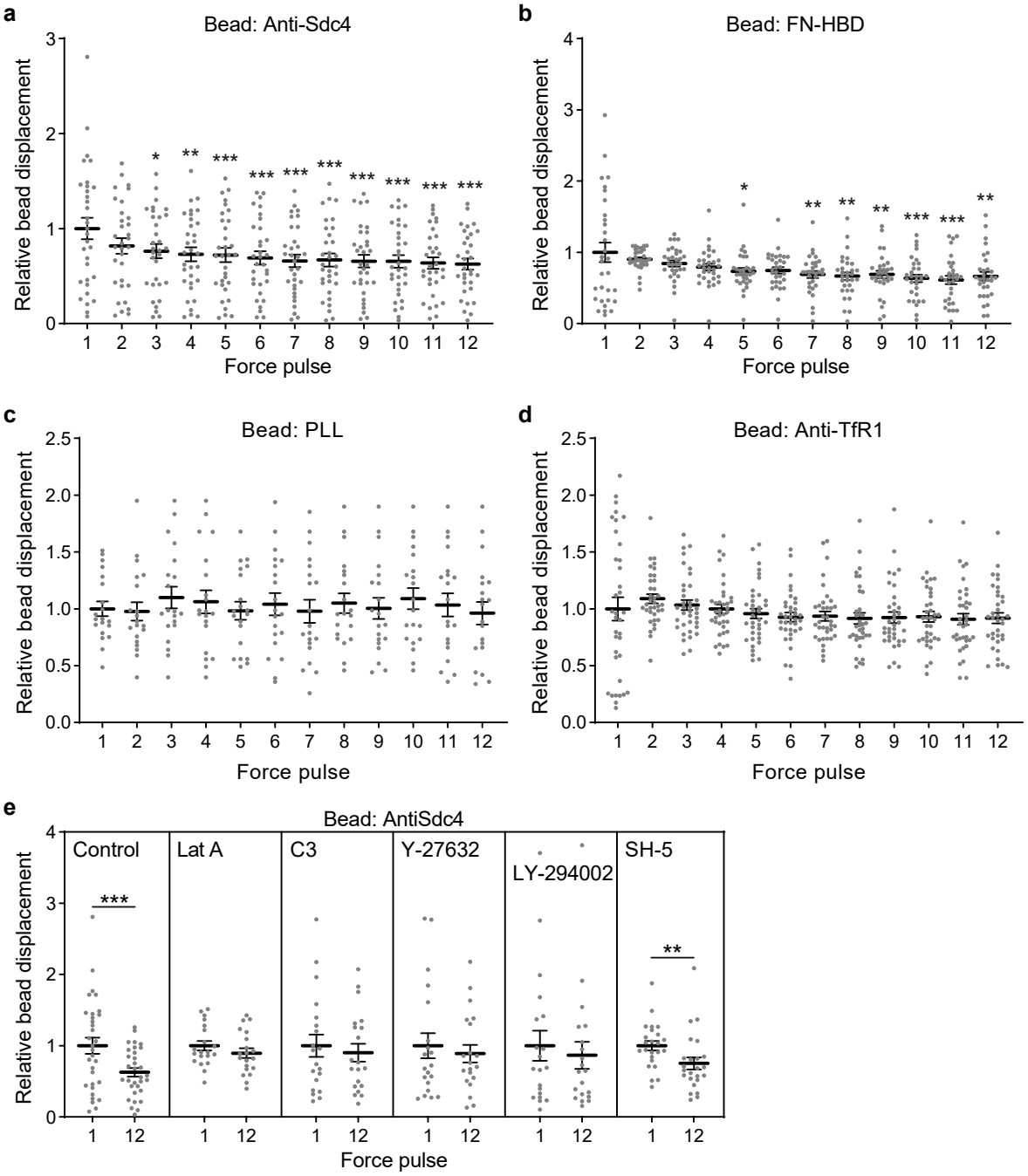

Supplementary Figure 4: Single cell data corresponding to summarised magnetic tweezers bead displacement data presented in Figure 1. Magnetic bead displacement amplitude in response to a 1 nN pulsatile force is presented for each pancreatic stellate cell (PSC) relative to the average first pulse displacement. **a-d,** Beads were functionalised with (**a**) mouse anti-syndecan-4 ectodomain antibody (Anti-Sdc4; $n = 32$), (**b**) the heparin binding domain fragment of fibronectin (FN-HBD; $n = 31$), (**c**) poly-L-lysine (PLL; $n = 20$), and (**d**) mouse anti-transferrin receptor protein-1 (Anti-TfR1; $n = 36$ cells). Friedman test with Dunn pairwise comparisons: $^{*}P \leq 0.0116$, $^{**}P \leq 0.0041$, $^{***}P < 0.0001$ vs force pulse 1. **e,** Single cell data for relative magnetic bead displacement at force pulse 1 and 12 for Anti-Sdc4 magnetic beads bound to untreated control PSCs ($n = 32$) or PSCs treated with F-actin polymerisation inhibitor latrunculin A (Lat A; 0.5 μM, 1 h; $n = 20$), Rho inhibitor C3 transferase (C3; 2 μg/mL, 4 h; $n = 20$), Rho-associated protein kinase (ROCK) inhibitor Y-27632 (10 μM, 1 h, $n = 20$), phosphoinositide 3-kinase (PI3K) inhibitor LY-294002 (30 μM, 1 h; $n = 20$), or AKT inhibitor SH-5 (10 μM, 1 h; $n = 24$ cells). Two-sided paired signed rank test: $^{**}P = 0.002$, $^{***}P < 0.0001$. Grey dots represent individual bead displacements, mean and s.e.m. overlaid.

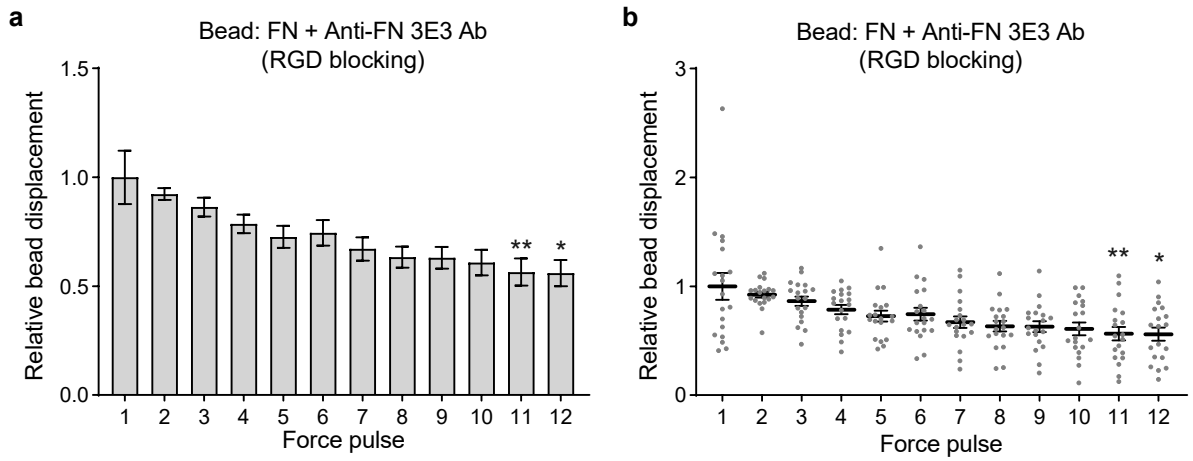

Supplementary Figure 5: Force applied to syndecan heparan sulphate chains induces adaptive cell stiffening. a,b, Magnetic bead displacement amplitude in response to a 1 nN pulsatile force is presented as summarised mean value (**a**) and for each pancreatic stellate cell (**b**) relative to the average first pulse displacement. Beads were functionalised with fibronectin treated with an RGD integrin binding site blocking antibody (clone 3E3) which leaves the heparin binding domain available (FN + Anti-FN 3E3 Ab; *n* = 19 cells). Friedman test with Dunn pairwise comparisons: **P* = 0.0104, ***P* = 0.0054 vs force pulse 1. Mean ± s.e.m. with individual values overlaid.

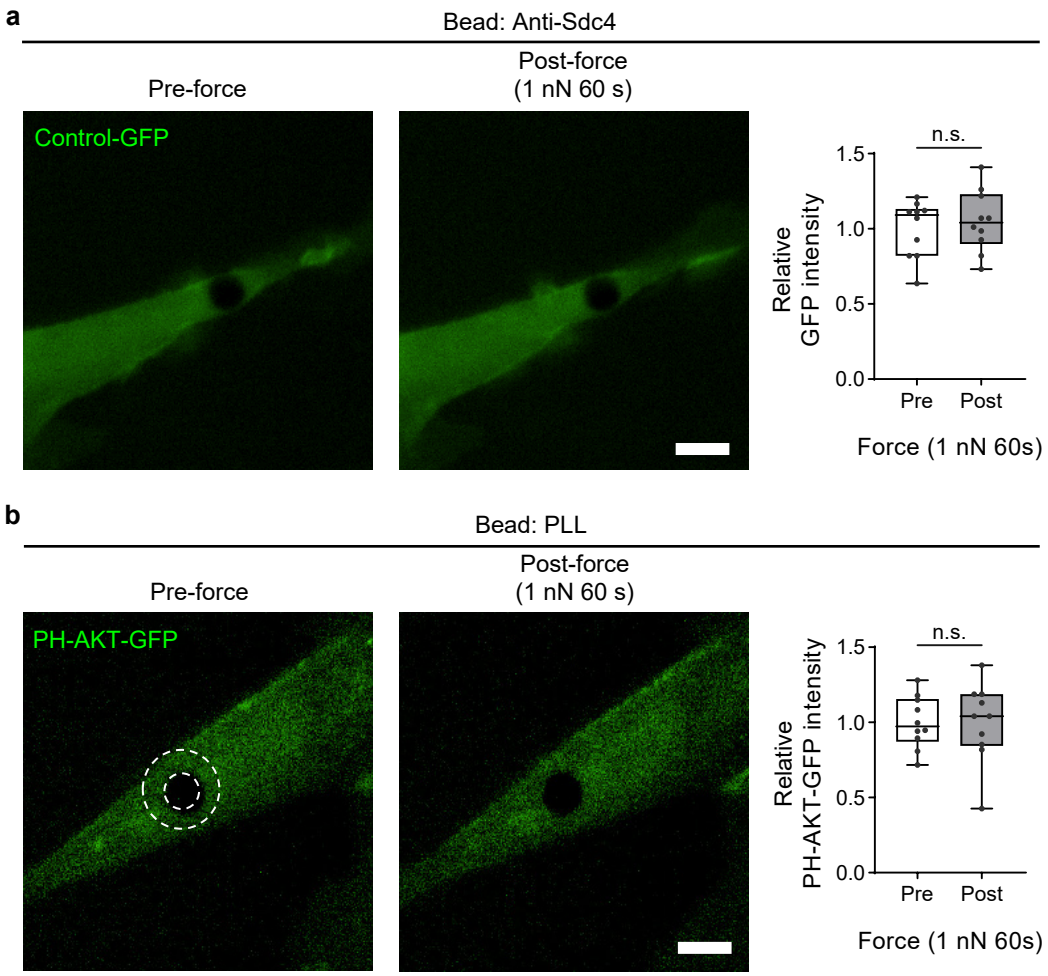

Supplementary Figure 6: Confirmation of specificity of force induced PI3K activation to syndecan-4. a, Sustained force applied to syndecan-4 bound beads on pancreatic stellate cells expressing an empty control GFP vector did not lead to GFP accumulation in the bead region, unlike in cells expressing the PIP_3 biosensor PH-AKT-GFP (Fig. 1e). **b,** Sustained force applied to poly-L-lysine (PLL) coated beads attached to cells expressing PH-AKT-GFP did not lead to PH-AKT-GFP accumulation at the bead; indicating that force-induced PI3K activation is specific to syndecan-4. Cells expressing either vector were exposed to a sustained tensional force of 1 nN for 60 s. Representative images of the area surrounding the magnetic bead pre (0 s) and post (60 s) force application. Mean PH-AKT-GFP fluorescent intensity, in a region of interest surrounding the bead depicted by white dashed overlay, is presented relative to mean intensity prior to force application. Scale bar: 5 μm. *n* = 10 cells from 2 biologically independent experiments; two-sided paired signed rank test: (a) n.s. *P* = 0.655, (b) n.s. *P* = 0.987. Boxes represent median and interquartile range, whiskers extend to the max/min data points, individual values are overlaid.

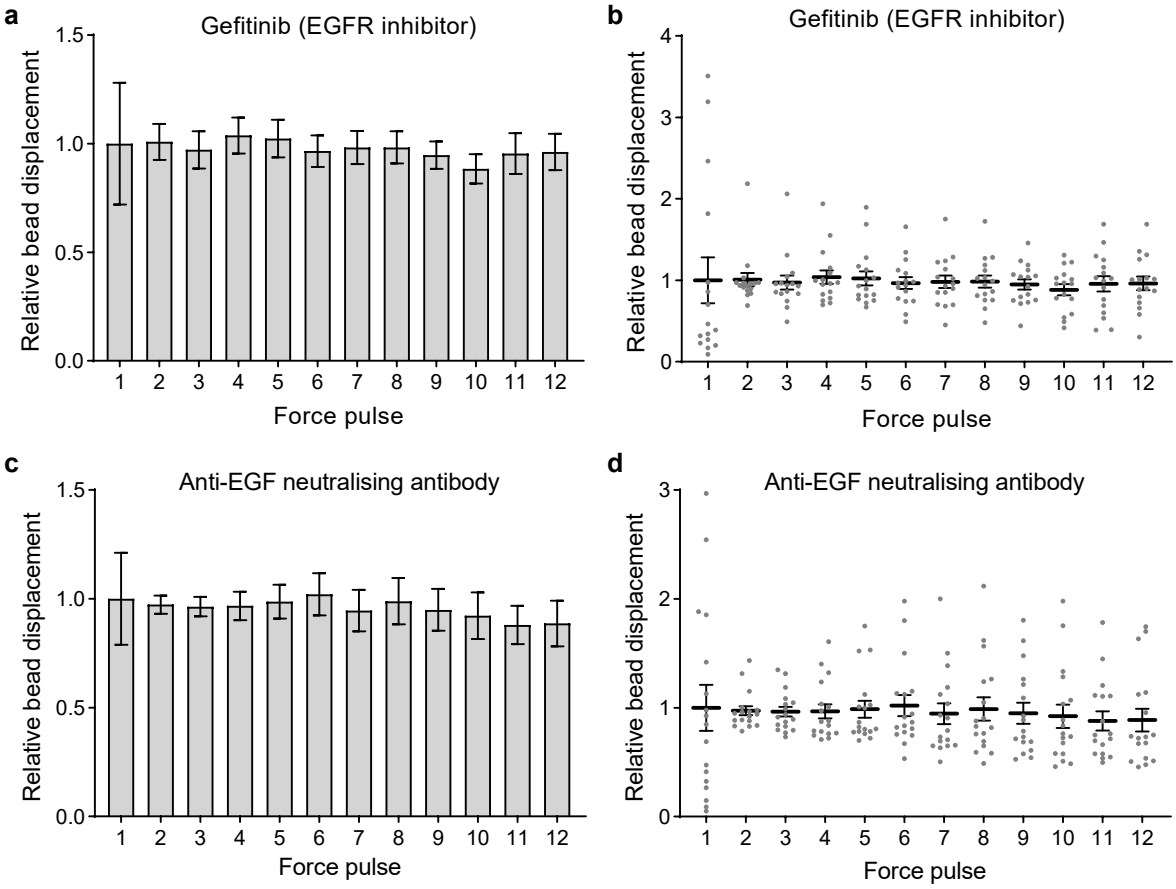

Supplementary Figure 7: EGFR is required for syndecan-4 mediated adaptive cell stiffening. Pulsatile force applied to syndecan-4 bound beads in the presence of **a,b,** Epidermal growth factor receptor (EGFR) inhibitor Gefitinib (Santa Cruz Biotechnology sc-202166, 15 μM, 2h; *n* = 16 cells) or **c,d**, anti-epidermal growth factor (EGF) neutralising antibody (R&D Systems MAB236, 5 μg ml^{-1}, 30 min; *n* = 17 cells) did not induce an adaptive stiffening response. Magnetic bead displacement amplitude in response to a 1 nN pulsatile force is presented as mean (**a**,**c**) and for each pancreatic stellate cell (**b**,**d**) relative to the average first pulse displacement. Beads were functionalised with mouse anti-syndecan-4 ectodomain antibody. Mean ± s.e.m. with individual values overlaid.

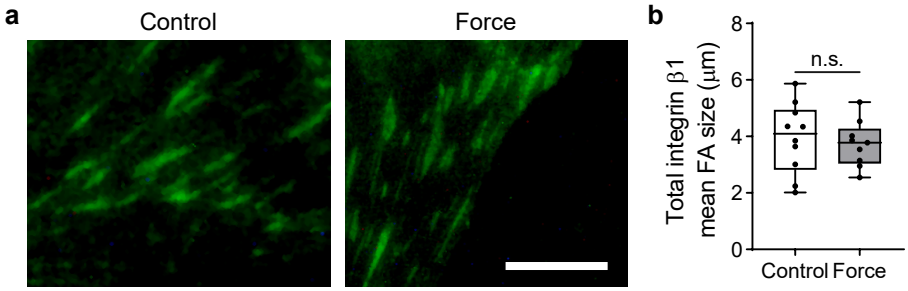

Supplementary Figure 8: Total integrin β1 incorporation into focal adhesions does not change in response to tension on syndecan-4. a, Representative epifluorescent microscopy images of total integrin β1 at the basal surface of pancreatic stellate cells in control conditions or in response to a sustained tensional force of approx. 200 pN for 5 min applied using a permanent magnet. Cells were fixed immediately post force application and immunofluorescently stained for integrin β1. Scale bar 5 μm. **b,** Quantification of mean focal adhesion size for integrin β1 containing adhesions. The mean adhesion size from > 10 focal adhesions from 3 regions of interest per cell are presented. $n_{Control}$ = 10 cells, n_{Force} = 9 cells; two-sided two-sample t-test: n.s. P = 0.678. Boxes represent median and interquartile range, whiskers extend to the max/min data points, with mean cell values overlaid.

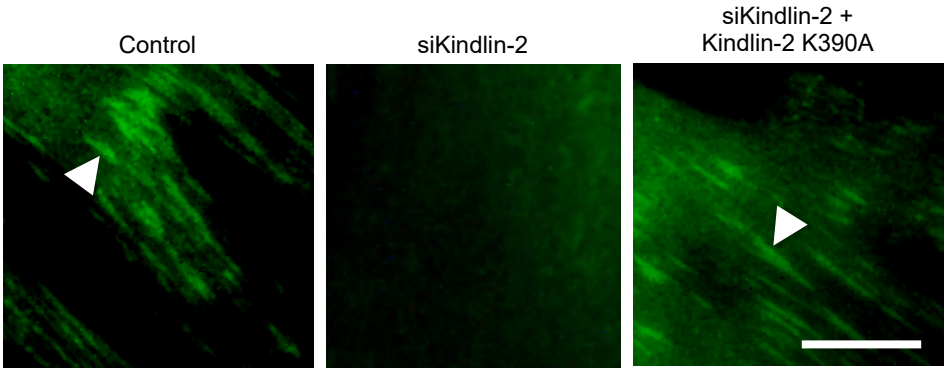

Supplementary Figure 9: Immunofluorescent staining demonstrating knockdown and re-expression of kindlin-2. Representative epifluorescent microscopy images of kindlin-2 at the basal surface of pancreatic stellate cells. Cells were left untreated (Control), treated with siRNA targeting kindlin-2 (siKindlin-2), and subsequently transfected with a plasmid to re-express a kindlin-2 mutant (K390A) lacking phosphoinositide binding activity (siKindlin-2 + Kindlin-2 K390A). Cells were fixed and immunofluorescently stained for kindlin-2. White arrowheads indicate incorporation of kindlin-2 in focal adhesions with no kindlin-2 positive adhesions observed in the siKindlin-2 condition. Representative images from 2 independent repeat experiments. Scale bar 5 μm.

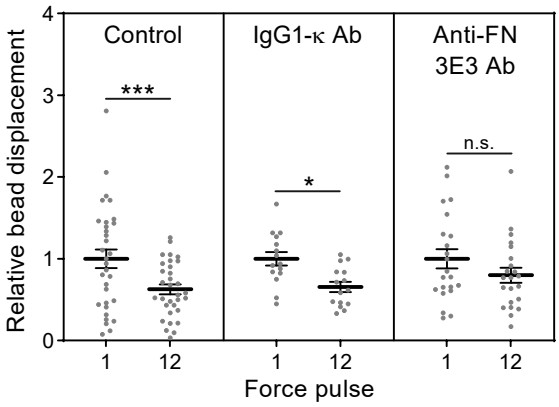

Supplementary Figure 10: Single cell data corresponding to summarised magnetic tweezers bead displacement data presented in Figure 4b. Bead displacement presented relative to the mean value for force pulse 1. Pulsatile force applied to syndecan-4 bound beads on pancreatic stellate cells plated on fibronectin in untreated control conditions (n = 32), in the presence of isotype control mouse IgG1-κ antibody (clone MOPC-21, Merck MABF1081Z; n = 15), and in the presence of mouse anti-fibronectin antibody (clone 3E3, Merck MAB88916-C), which blocks the RGD integrin binding site of fibronectin preventing new integrin-RGD connections (n = 22 cells). Both antibodies were added at 20 μg ml^{-1} for 30 min prior to initiation of magnetic tweezer stimulation and were maintained throughout experiments. Two-sided paired signed rank test: *P = 0.035, ***P < 0.0001, n.s. P = 0.134. Mean ± s.e.m. with individual values overlaid.

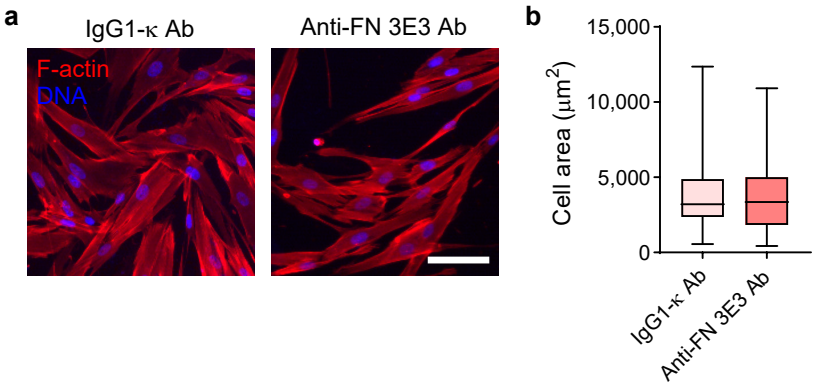

Supplementary Figure 11: Blocking of fibronectin's RGD binding site does not alter cell spread area. a, Representative epifluorescent microscopy images of f-actin in pancreatic stellate cells in the presence of isotype control mouse IgG1-κ antibody (clone MOPC-21, Merck MABF1081Z) or mouse anti-fibronectin antibody (clone 3E3, Merck MAB88916-C), which blocks the RGD integrin binding site of fibronectin preventing new integrin-RGD connections. Both antibodies were added at 20 μg ml^{-1} for 30 min prior to fixation of cells. Scale bar 100 μm. **b,** Quantification of cell spread area corresponding to images in (**a**). Morphological outlines were manually traced on F-actin overlays in ImageJ. $n_{IgG1\text{-}\kappa}$ = 142 cells, $n_{Anti\text{-}FN\ 3E3}$ = 91 cells; two-sided Mann-Whitney test: P = 0.416. Boxes represent median and interquartile range, whiskers extend to the max/min data points.

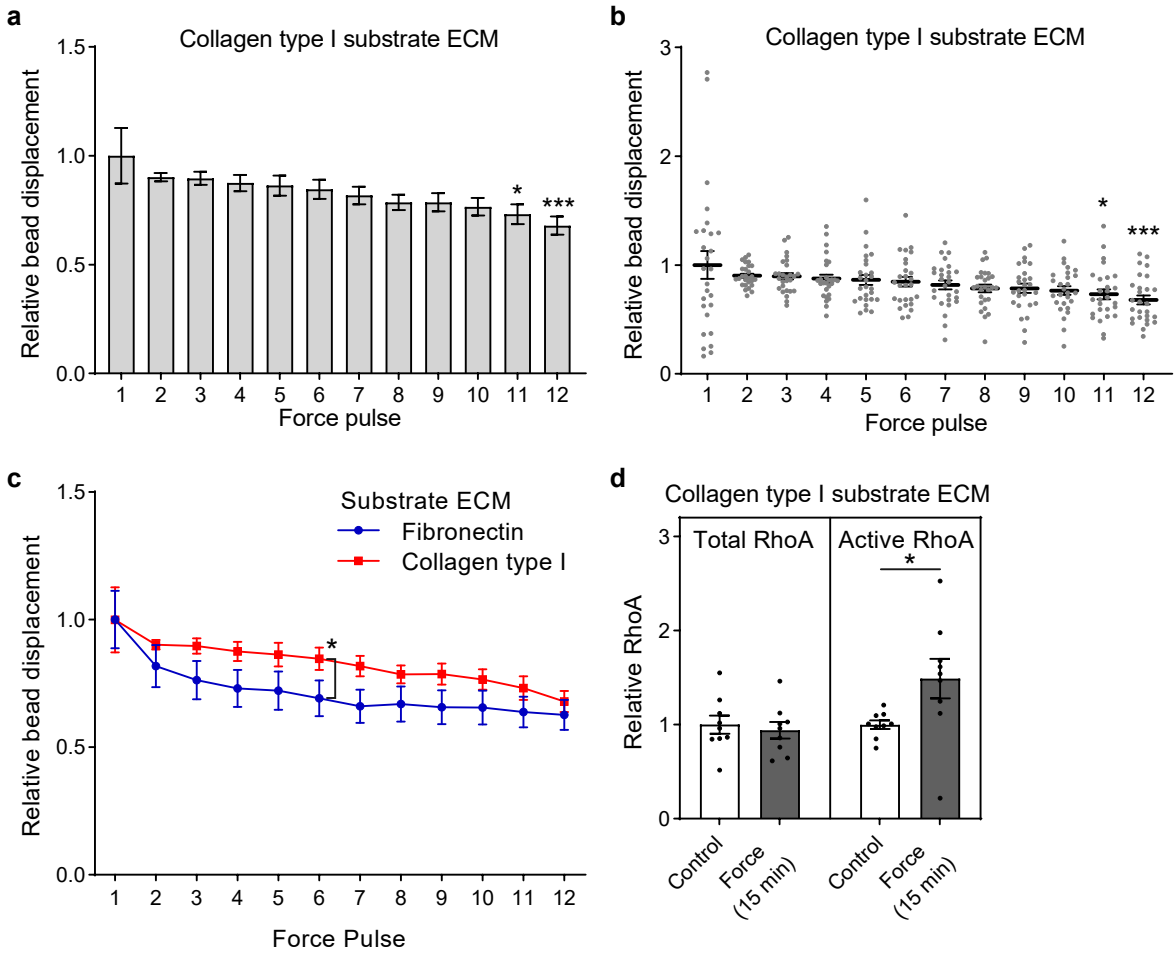

Supplementary Figure 12: Syndecan-4 tension mediated cell stiffening and RhoA activation persists in cells seeded on collagen type I. a,b, 1 nN pulsatile force was applied to syndecan-4 bound beads on pancreatic stellate cells (PSCs) plated on collagen type I. Mean (**a**) and individual cell (**b**) bead displacement presented relative to the average displacement of force pulse 1. n = 27 cells; Friedman test with Dunn pairwise comparisons: *P = 0.0179, ***P = 0.0007 vs force pulse 1. **c,** Relative syndecan-4 bound bead displacement for PSCs plated on fibronectin (n = 32, see Supplementary Fig. 3) and on collagen as presented in (**a**,**b**). The reduction in bead displacement with each force pulse is less rapid in cells on collagen compared to cells on fibronectin. $n_{Fibronectin}$ = 32, $n_{Collagen\ type\ I}$ = 27 cells; two-sided two sample t-test: *P = 0.046. **d,** Syndecan-4 bound beads on PSCs plated on collagen type I were subjected to sustained tension of ~200 pN for 15 min, with total and active RhoA assessed using ELISA and G-LISA respectively, presented relative to unstimulated control. The application of sustained force led to an increase in RhoA activation, but this was less marked as that in cells on fibronectin (Fig. 4a). n = 9 biologically independent samples; two-sided two-sample t-test: *P = 0.037. Mean ± s.e.m. with individual values overlaid.

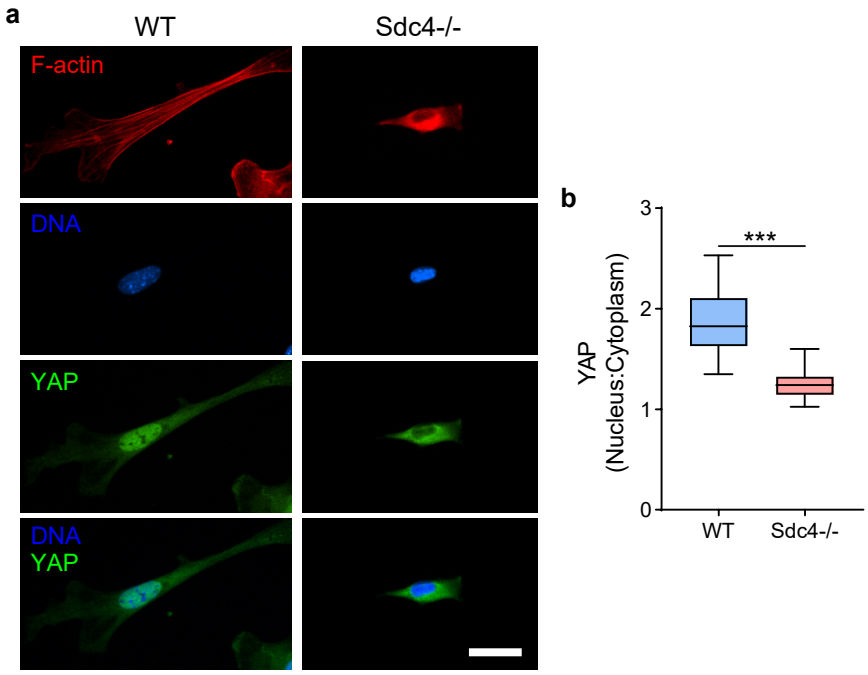

Supplementary Figure 13. Syndecan-4 is required for YAP nuclear localisation on fibronectin coated 25 kPa gels. a, Wild type (WT) and syndecan-4 null (Sdc4-/-) mouse embryonic fibroblasts were plated onto fibronectin coated 25 kPa polyacrylamide gels, fixed and immunofluorescently stained for YAP. Representative wide field microscopy images for DNA, F-actin and YAP. Scale bar 20 μm. **b,** Quantification of mean nuclear:cytoplasmic YAP intensity. n_{WT} = 18, $n_{Sdc4-/-}$ = 16 cells; two-sided two-sample t-test: ***$P < 0.0001$. Boxes represent median and interquartile range, whiskers extend to the max/min data points.

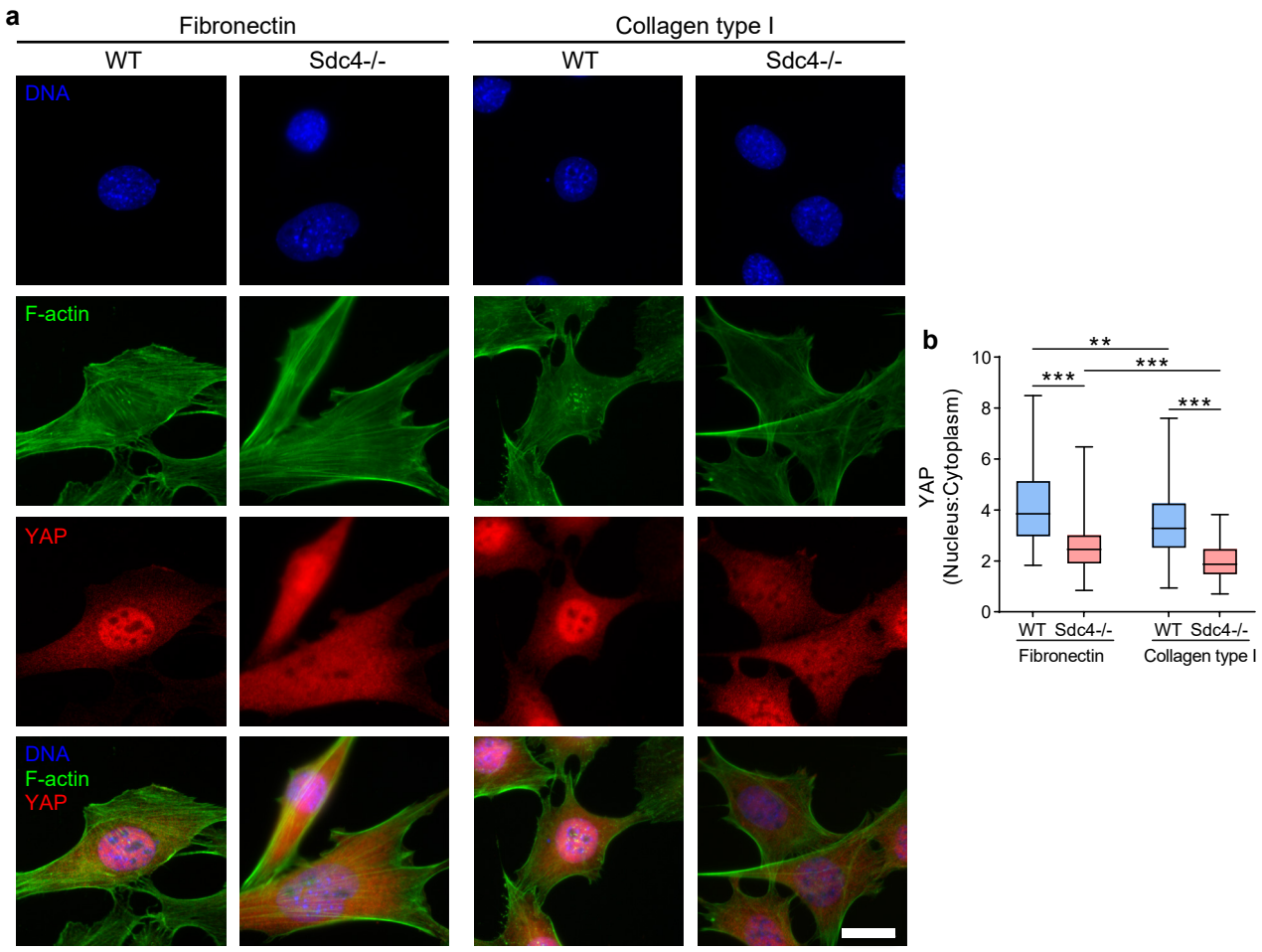

Supplementary Figure 14: Syndecan-4 is required for YAP nuclear translocation in mouse embryonic fibroblasts plated on fibronectin or collagen type I. Wild type (WT) and syndecan-4 null (Sdc4-/-) mouse embryonic fibroblasts were plated on fibronectin or collagen type I coated substrates. **a,** Representative epifluorescent microscopy images for DNA, F-actin, YAP and merged channels. Scale bar 20 μm. **b,** Quantification of mean nuclear:cytoplasmic YAP intensity. $n_{Fibronectin\text{-}WT}$ = 96, $n_{Fibronectin\text{-}Sdc4\text{-}/\text{-}}$ = 82, $n_{Collagen\ 1\text{-}WT}$ = 91, $n_{Collagen\ 1\text{-}Sdc4\text{-}/\text{-}}$ = 172 cells; two-sided Mann-Whitney tests: $^{**}P = 0.005$, $^{***}P < 0.001$. Boxes represent median and interquartile range, whiskers extend to the max/min data points. YAP downregulation in Sdc4-/- cells was not affected by substrate ECM with Sdc4-/- cells on collagen type I exhibiting a reduction in nuclear YAP compared to WT. Both WT and Sdc4-/- cells exhibited decreased nuclear:cytoplasmic YAP on collagen type I compared to fibronectin.

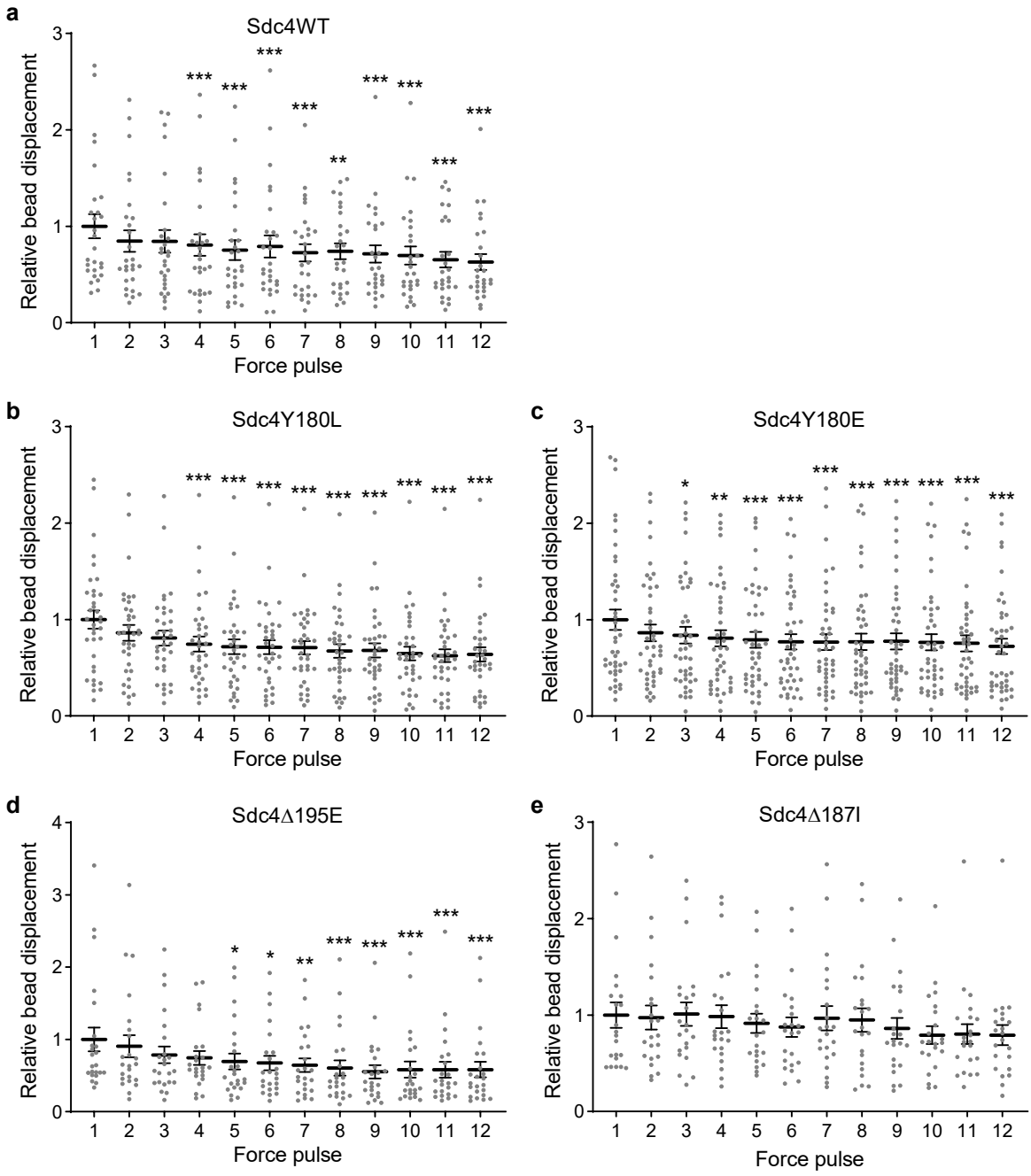

Supplementary Figure 15: Single cell data corresponding to summarised magnetic tweezers bead displacement data presented in Figure 5c. a-e, Bead displacement presented relative to the mean value for force pulse 1 in response to 1 nN pulsatile force applied to syndecan-4 bound beads on mouse embryonic fibroblasts (MEFs) plated on fibronectin. MEF cell lines expressing (**a**) wild type syndecan-4 (Sdc4WT; *n* = 27), (**b**) phospho-null syndecan-4 (Sdc4Y180L; *n* = 35), (**c**) phospho-mimetic syndecan-4 (Sdc4Y180E; *n* = 43), (**d**) syndecan-4 truncated in the C2 domain (Sdc4Δ195E; *n* = 23), or (**e**) syndecan-4 truncated in the variable (V) domain (Sdc4Δ187I; *n* = 22 cells). Friedman test with Dunn pairwise comparisons: **P* ≤ 0.0238, ***P* ≤ 0.0092, ****P* ≤ 0.001 vs force pulse 1. Mean ± s.e.m. with individual values overlaid.

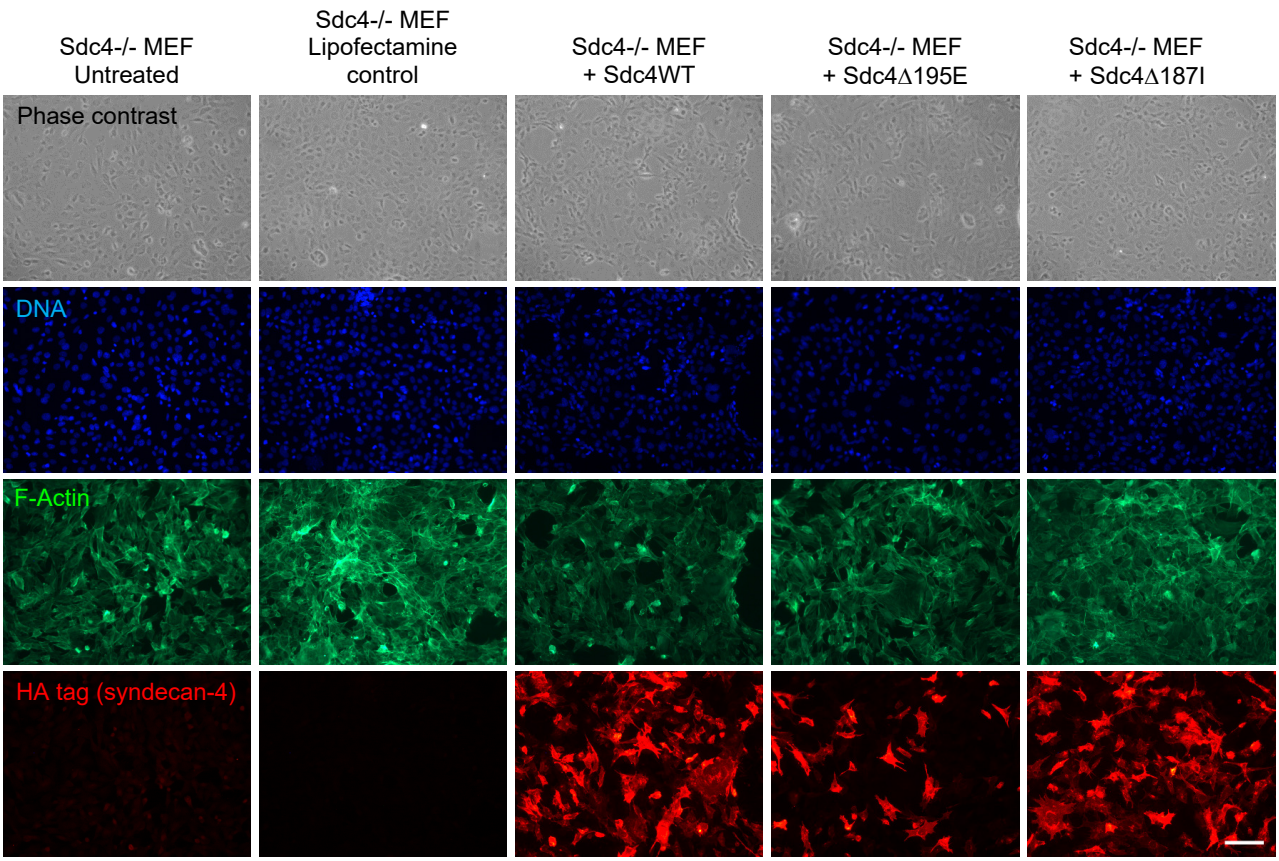

Supplementary Figure 16: Confirmation of syndecan-4 plasmid transfection into syndecan-4 null (Sdc4-/-) mouse embryonic fibroblast (MEF) line. Representative epifluorescent microscopy images of immunofluorescent staining for F-actin and HA tagged syndecan-4 plasmid expression. Sdc4-/- MEFs expressing wild type syndecan-4 (Sdc4WT), syndecan-4 truncated in the C2 domain (Sdc4Δ195E), or syndecan-4 truncated in the variable domain (Sdc4Δ187I) were fixed 24 h post transfection. Images are representative from 2 biologically independent experiments with similar results. Scale bar 100 μm.

a

MAPARLFALL LFFVGGVAES IRETEVIDPQ DLLEGRYFSG 40
ALPDDEDVVG PGQESDDFEL SGSGDLDDLE DSMIGPEVVH 80
PLVPLDNHIP ERAGSGSQVP TEPKKLEENE VIPKRISPVE 120
ESEDVSNKVS MSSTVQGSNI FERTEVLAAL IVGGIVGILF 160
AVFLILLLMY RMKKKDEGSY DLGKKPIYKK APTNEFYA 198

C1 region Variable region C2 region

Signal peptide
Extracellular domain
Transmembrane domain
Cytoplasmic domain (C1, Variable and C2 regions)
Sequence included in the simulations

b

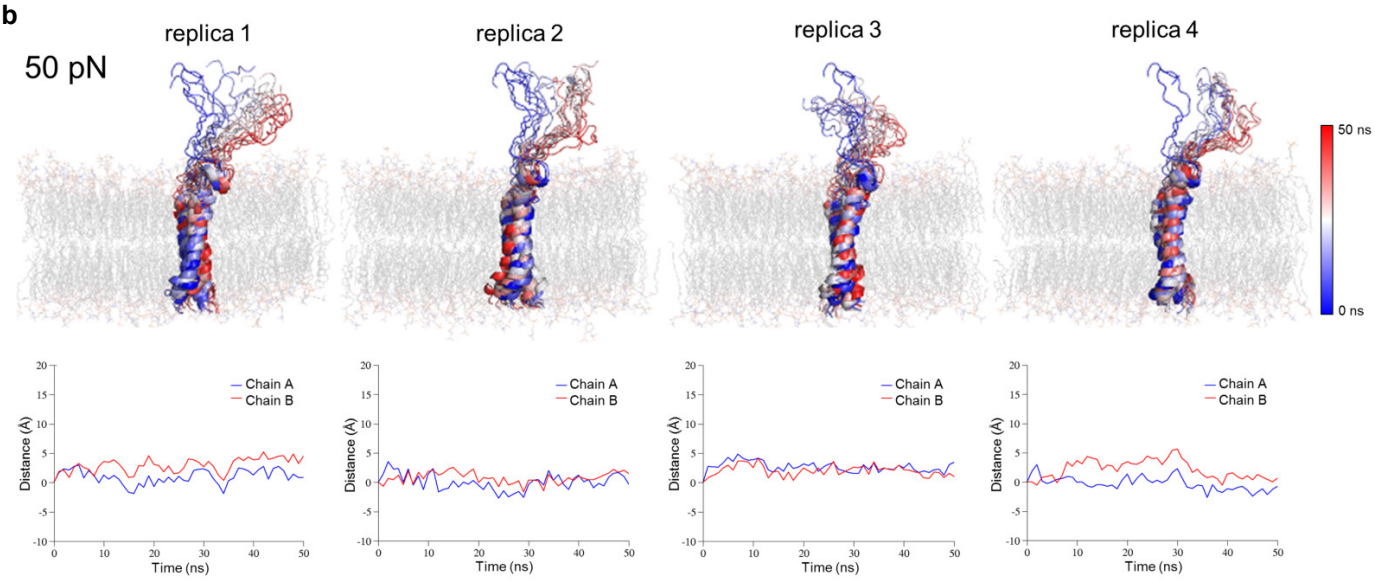

Supplementary Figure 17: Steered molecular dynamics (SMD) simulations reveal conformational changes in the cytoplasmic domain of syndecan-4 in response to force on the extracellular domain. a, Syndecan-4 amino acid sequence, where 1-18: signal peptide, 19-145: extracellular domain (green), 146-170: transmembrane domain (brown), 171-198: cytoplasmic domain (purple). Region used in molecular dynamics (MD) and steered molecular dynamics (SMD) simulations is underlined. **b,** Multiple replica SMD simulations at 50 pN. Conformational changes of the cytoplasmic domain of syndecan-4 (upper panel) and sliding of syndecan-4 through the membrane (lower panel) in steered molecular dynamics (SMD) simulations using constant force pulling at 50 pN for 50 ns (4 parallel simulations).

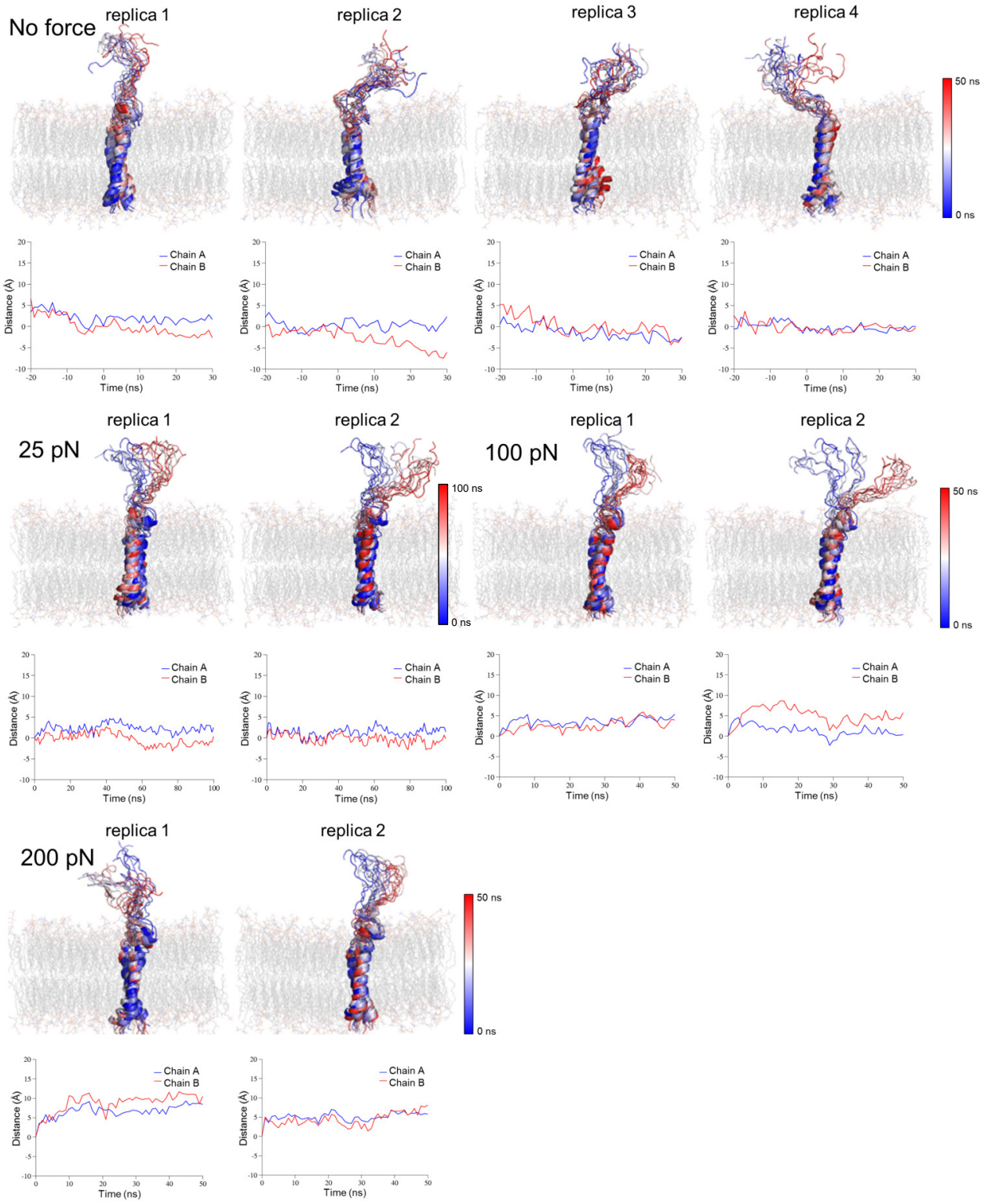

Supplementary Figure 18: Effect of force magnitude on syndecan-4 conformation in molecular dynamics (MD) and steered molecular dynamics (SMD) simulations. Conformational changes of cytoplasmic domain of syndecan-4 (upper panel) and sliding of syndecan-4 through the membrane (lower panel) in MD over 50 ns (No force; 4 parallel simulations) and SMD simulations using constant force pulling at 25 pN for 100 ns (2 parallel simulations), 100 pN for 50 ns (2 parallel simulations) and 200 pN for 50 ns (2 parallel simulations).

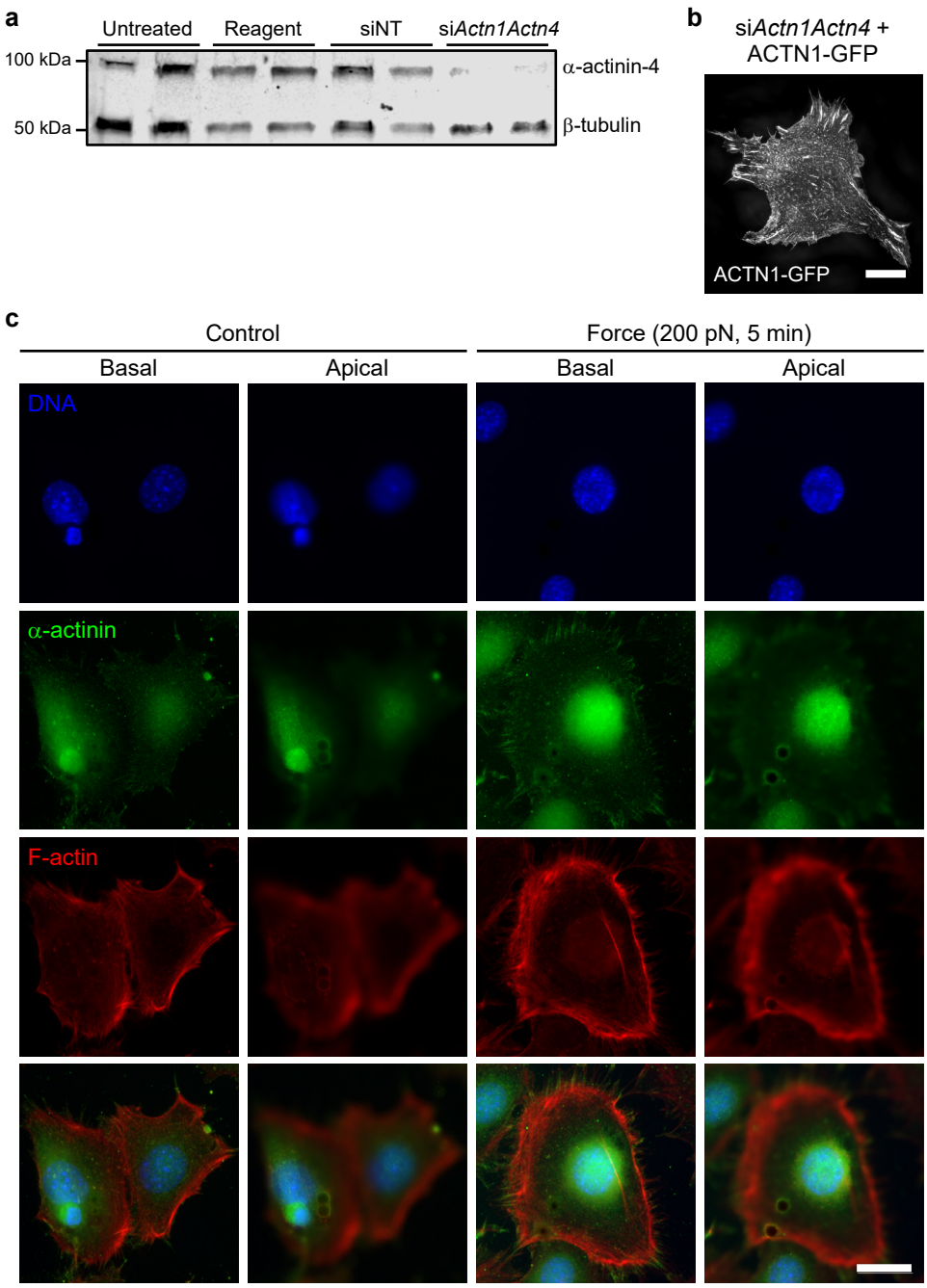

Supplementary Figure 19: α-actinin-1-GFP localises to focal adhesions akin to endogenous α-actinin. a, Western blot demonstrating successful siRNA mediated knockdown of α-actinin-4. Mouse embryonic fibroblasts (MEFs) were untreated, treated with transfection reagent lipofectamine 3000 alone, with a non-targeting control siRNA (siNT), and siRNAs targeting both α-actinin-1 (*Actn1*) and α-actinin-4 (*Actn4*; si*Actn1Actn4*). Duplicate samples presented are representative from 2 biologically independent experiments with similar results. **b,** Representative maximum projection of a 3D super resolution structured illumination microscopy image of α-actinin-1-GFP (ACTN1-GFP) localisation in *Actn1* and *Actn4* depleted MEFs. Note intense localisation to focal adhesions. Image representative of 3 biologically independent experiments with similar results. Scale bar 10 μm. **c,** Representative wide field immunofluorescent images of DNA, F-actin and α-actinin in pancreatic stellate cells under control unstimulated conditions, and in response to sustained 200 pN force for 5 min applied using a permanent magnet to syndecan-4 bound beads. Images were taken at the basal and apical (bead) plane. Note the localisation of α-actinin around the bead adhesion. Images representative of 2 independent experiments with similar results. Scale bar 20 μm.

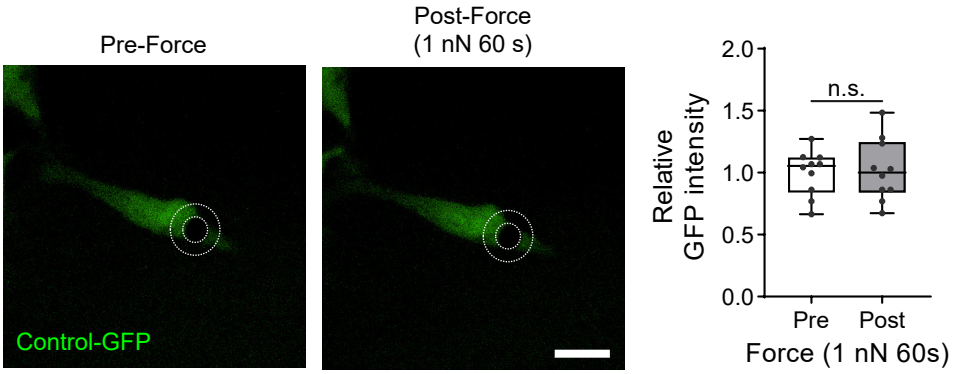

Supplementary Figure 20: Force on syndecan-4 bound beads does not induce control empty vector GFP accumulation in the bead region. Sustained force of 1 nN for 60 s applied to syndecan-4 bound beads on mouse embryonic fibroblasts expressing an empty control GFP vector did not lead to GFP accumulation in the bead region, unlike in cells expressing α-actinin-1 (ACTN1)-GFP (Fig. 6b). Representative images of the area surrounding the magnetic bead pre (0 s) and post (60 s) force application. Mean GFP fluorescent intensity, in a region of interest surrounding the bead depicted by white dashed overlay, is presented relative to mean intensity prior to force application. Scale bar: 10 μm. *n* = 10 cells; two-sided paired signed rank test: n.s. *P* = 0.754. Boxes represent median and interquartile range, whiskers extend to the max/min data points, individual values are overlaid.

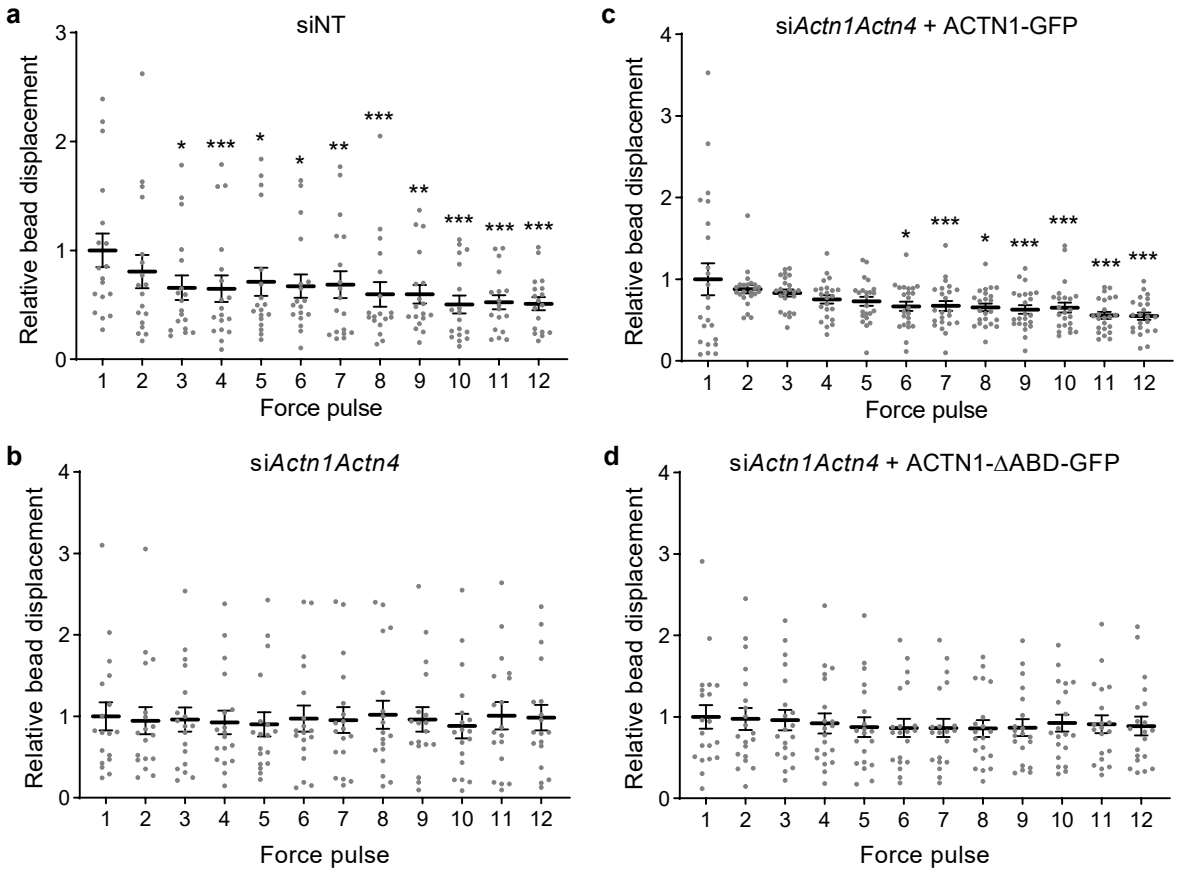

Supplementary Figure 21: Single cell data corresponding to summarised magnetic tweezers bead displacement data presented in Figure 6d. a-d, Bead displacement presented relative to the mean value for force pulse 1 in response to 1 nN pulsatile force applied to syndecan-4 bound beads on mouse embryonic fibroblasts (MEFs) plated on fibronectin. MEFs were treated with (**a**) non-targeting control siRNA (siNT; *n* = 18) or (**b**) siRNAs targeting α-actinin-1 (*Actn1*) and α-

actinin-4 (*Actn4*; si*Actn1Actn4*; *n* = 18) with expression of (**c**) α-actinin-1 (ACTN1)-GFP (si*Actn1Actn4* + ACTN1-GFP; *n* = 23) or (**d**) a mutant form of α-actinin with the actin binding domain (ABD) deleted (si*Actn1Actn4* + ACTN1-ΔABD-GFP; *n* = 20 cells).; Friedman test with Dunn pairwise comparisons: **P* ≤ 0.0492, ***P* ≤ 0.0058, ****P* ≤ 0.0009 vs force pulse 1. Mean ± s.e.m. with individual values overlaid.

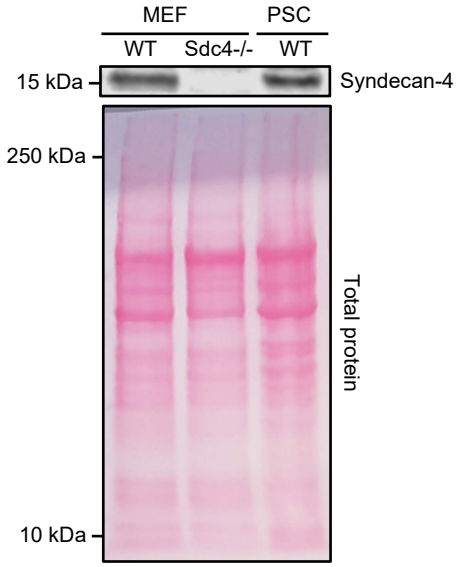

Supplementary Figure 22: Syndecan-4 is expressed in wild type (WT) mouse embryonic fibroblasts (MEFs) and pancreatic stellate cells (PSCs) but not in syndecan-4 null (Sdc4-/-) MEFs. Western blot bands for syndecan-4 (Sdc4) and Ponceau-S staining for total protein. Blot representative of 3 independent experimental repeats with similar results. Full syndecan-4 blot is presented in Supplementary Fig. 23.

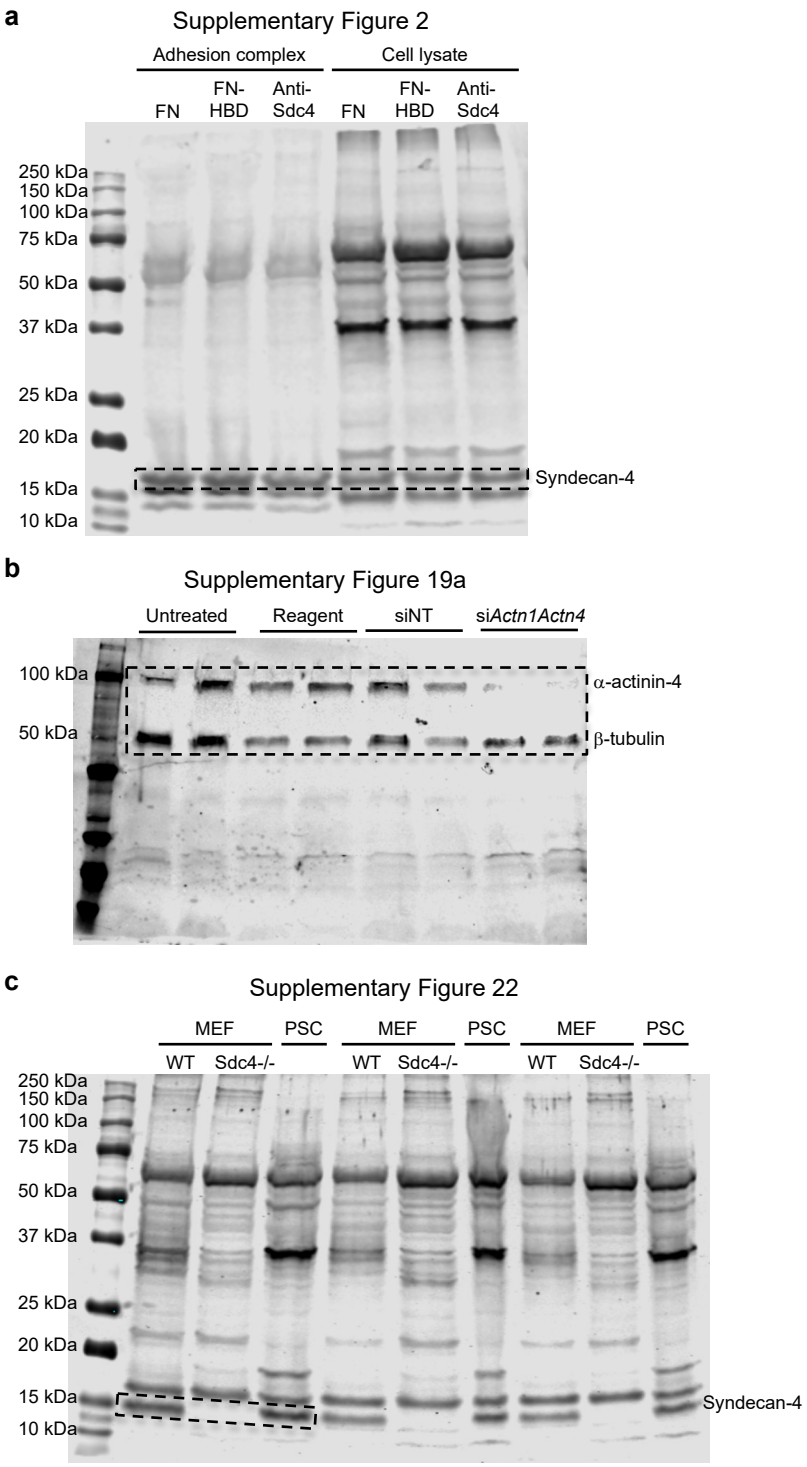

Supplementary Figure 23: Full blot membranes for western blot bands. a-c, Full blot membranes for bands presented in (**a**) Supplementary Fig. 2, (**b**) Supplementary Fig. 19a, and (**c**) Supplementary Fig. 22. In order to resolve syndecan-4 in western blots, heparan sulphate chains were removed through heparinase digestion. Regions presented in respective figures are identified by dashed box.

Supplementary Discussion

Cell-wide integrin activation is triggered by PI3K and leads to subsequent production of freely diffusible PIP_3 phosphoinositides that bind to the PH domain of focal adhesion protein kindlin-2, switching β1 integrins into a high affinity state to promote ECM ligation. The diffusion rate of PIP_3 is ~0.1-1 $\mu m^2 s^{-1}$ (ref. 1), which is sufficient for the propagation of the biochemical signal to sites distal from that of force application to initiate global activation of integrins within the timescales of our experiments. It is therefore likely that the stiffening response to syndecan-4 mechanosensing represents a global cytoskeletal response rather than a local strengthening of the bead adhesion complex.

Molecular dynamics simulations of tension application to the extracellular domain of syndecan-4 revealed a force-dependent repositioning of the cytoplasmic domain where the V-region moved toward the plasma membrane. This mechanism contrasts with mechanotransduction mechanisms requiring mechanical unfolding of proteins to expose cryptic sites for signalling[2]. This conformation change may facilitate interaction between the V-region and membrane associated PIP_2 which is necessary for PKC-α activation[3], or facilitate α-actinin binding[4]. A direct interaction between the syndecan-4 V-region and α-actinin is a key functional unit that promotes the assembly of focal adhesions and their associated linear microfilament bundles[5]. We have found that force-induced stabilisation of a syndecan-4/α-actinin/F-actin molecular scaffold at the focal adhesion serves as a direct structural link to the cytoskeleton necessary for force transmission and downstream mechanosignalling. α-actinin also associates with integrins, vinculin and zyxin within focal adhesions. It may also possess signalling roles as reports indicate α-actinin interacts with PIP_2 and focal adhesion kinase (FAK)[6]. Force-induced stabilisation of α-actinin at syndecan-4 enriched adhesions may result in recruitment of other essential adhesion components such as zyxin, vinculin and β1 integrins, to establish cell contraction and downstream syndecan-4 mechanosignalling. Beyond its function to sustain tension across syndecan-4 adhesions, α-actinin may also have direct additional roles in signalling, or indirectly as a force-sensitive scaffold via recruitment of other signalling proteins.

Syndecan-4-mediated force transduction was also found to activate YAP, a major transcriptional regulator and mechanosensor that relays mechanical and cytoskeletal signals to the nucleus. We demonstrate that syndecan-4-mediated tension at the cell-ECM interface is required for nuclear shuttling and activation of YAP and subsequent transcription of downstream YAP target genes. Low matrix tension or attenuated syndecan-4 mechanosignalling causes cytoplasmic YAP retention. The fact that the syndecan-4 null phenotype displays largely deactivated YAP and repressed YAP transcriptional signalling indicates a requirement for ECM ligation and mechanosignalling via both integrins and syndecan-4 to fully activate YAP. The syndecan-4 null phenotype has a distinct cytoskeletal architecture with defects in microfilament assembly and an absence of F-actin stress fibres[5,7], as well as impairments in focal adhesion assembly[5,8]. Presumably, deactivated YAP in syndecan-4 null cells is secondary to lower cytoskeletal tension, owing to deficits in F-actin stress fibre formation and destabilisation of cell-matrix adhesions resulting in decreased RhoA signalling and YAP activity.

Interestingly, a recent study demonstrated a direct kindlin-2-RhoA signalling axis that senses mechanical cues from the cell microenvironment to control YAP and mesenchymal stem cell differentiation[9]. Since syndecan-4 knockout also results in phenotypic disturbances and secondary cytoskeletal impairments[5], we speculate that the mechanical activation of YAP downstream of syndecan-4 may be linked to a RhoA-mediated increase in overall cytoskeletal tension and stress fibre assembly, leaving the possibility for a similar kindlin-2-RhoA axis.

The broader implications for this force-dependent regulation of β1 integrin activity in stromal fibroblasts downstream of syndecan-4 have yet to be established but likely extend to other cellular processes. For example, fibronectin has binding sites for both integrins and syndecans and a growing body of studies has revealed actomyosin generated forces transmitted through members of the β1 integrin family play a critical role in fibronectin fibrillogenesis[10]. Also, syndecan family members have been shown to play a role in the architectural regulation of the matrix microenvironment, potentially creating favourable niches for directional migration and cancer metastasis[11]. Thus, stromal syndecan-4 mechanotransduction may modulate the program of fibronectin fibrillogenesis, matrix assembly and overall ECM organisation by regulating integrin-mediated adhesion and actomyosin contraction with important implications for connective tissue homeostasis in health and disease. A stiff fibrotic matrix is a major clinical finding in most solid tumours. While the role of integrin-mediated mechanosignalling has been the subject of intense investigation in the field of cancer mechanobiology in recent years, a more integrative approach that includes syndecan-4 as a key mechanosensor could pave the way for novel insights into disease mechanisms.

Supplementary Methods

Western blotting

Immediately after treatment, cell lysates were prepared in radio immunoprecipitation assay (RIPA) buffer (Sigma-Aldrich R0278) containing protease inhibitors (Sigma-Aldrich 4693124001) and phosphatase inhibitors (Sigma-Aldrich 4906837001). Cell lysates were centrifuged at 16,000 ×g for 20 min, and protein concentration was quantified using a BCA protein assay kit (Fisher Scientific 10678484). In order to resolve syndecan-4 in western blots, heparan sulphate chains were removed through enzymatic digestion. 100 μg total protein was methanol precipitated and suspended in buffer containing 50 mM HEPES, 50 mM NaOAc, 150 mM NaCl, 5 mM $CaCl_2$, ph 6.5 with 4×10^{-3} IU ml^{-1} heparinase I and 2.6 IU ml^{-1} heparinase III (Sigma-Aldrich H3917) for 4 h at 37°C with gentle rotation. Lysate was mixed with 4× Laemmli sample buffer including β-mercaptoethanol, heated at 95°C for 5 min, and 10-20 μg loaded into each well of a 4-20% gel (Mini-PROTEAN TGX, Bio-Rad). For analysis of adhesion complex, cell lysates were prepared from 25 cm^2 flasks in 1% IGEPAL CA-630 (Sigma I8896), 150 mM NaCl, 50 mM Tris, pH 8 buffer containing EDTA-free protease inhibitors (Sigma 11836170001) and phosphatase inhibitors. Following rotation at 4°C for 25 min, beads were isolated from the cell lysate using a magnet. Beads were washed 3 times in lysis buffer and suspended in 2× Laemmli sample buffer containing β-mercaptoethanol, heated at 95°C for 5 min, and bead complex loaded into a 4-20% gel alongside whole cell lysate controls. Separated proteins were transferred onto nitrocellulose membrane (Bio-Rad). Total protein was assessed using Ponceau S stain (Sigma-Aldrich). Following removal of Ponceau S, blots were blocked in Odyssey Blocking Buffer in Tris buffered saline (TBS; Li-Cor) for 1 h. Blots were incubated with primary antibodies diluted in TBS-tween 20 (TBST) at 4°C overnight. Following washes in TBST, blots were incubated with IRDye 680RD or IRDye 800CW conjugated donkey anti-mouse or donkey anti-rabbit secondary antibodies (Li-Cor) at 1:15,000 in TBST for 1 h. After washing in TBST, blots were imaged using an Odyssey infrared imager. Quantification of protein bands was carried out using Image Studio Lite 5.2 (Li-Cor). Primary antibodies: rabbit anti-β-tubulin (1:5,000; Abcam ab15568; RRID:AB_2210952), mouse anti-α-actinin 4, clone G-4 (1:500, Santa Cruz Biotechnology sc-390205; RRID:AB_2797388) and rabbit anti-syndecan-4 (1:500 Abcam ab24511; RRID:AB_448112). Uncropped blots are presented in Supplementary Figure 23.

Supplementary References

1 Hammond, G. R., Sim, Y., Lagnado, L. & Irvine, R. F. Reversible binding and rapid diffusion of proteins in complex with inositol lipids serves to coordinate free movement with spatial information. *J Cell Biol* **184,** 297-308 (2009).

2 del Rio, A. *et al.* Stretching single talin rod molecules activates vinculin binding. *Science* **323,** 638-641 (2009).

3 Bass, M. D. & Humphries, M. J. Cytoplasmic interactions of syndecan-4 orchestrate adhesion receptor and growth factor receptor signalling. *Biochem. J.* **368,** 1-15 (2002).

4 Greene, D. K., Tumova, S., Couchman, J. R. & Woods, A. Syndecan-4 associates with alpha-actinin. *J. Biol. Chem.* **278,** 7617-7623 (2003).

5 Okina, E., Grossi, A., Gopal, S., Multhaupt, H. A. & Couchman, J. R. Alpha-actinin interactions with syndecan-4 are integral to fibroblast-matrix adhesion and regulate cytoskeletal architecture. *Int. J. Biochem. Cell Biol.* **44,** 2161-2174 (2012).

6 Sjoblom, B., Salmazo, A. & Djinovic-Carugo, K. Alpha-actinin structure and regulation. *Cell Mol Life Sci* **65,** 2688-2701 (2008).

7 Gopal, S. *et al.* Heparan sulfate chain valency controls syndecan-4 function in cell adhesion. *J. Biol. Chem.* **285,** 14247-14258 (2010).

8 Cavalheiro, R. P. *et al.* Coupling of vinculin to F-actin demands Syndecan-4 proteoglycan. *Matrix Biol.* **63,** 23-37 (2017).

9 Guo, L. *et al.* Kindlin-2 regulates mesenchymal stem cell differentiation through control of YAP1/TAZ. *J Cell Biol* **217,** 1431-1451 (2018).

10 Schwarzbauer, J. E. & DeSimone, D. W. Fibronectins, their fibrillogenesis, and in vivo functions. *Cold Spring Harb Perspect Biol* **3,** 1-19 (2011).

11 Yang, N., Mosher, R., Seo, S., Beebe, D. & Friedl, A. Syndecan-1 in breast cancer stroma fibroblasts regulates extracellular matrix fiber organization and carcinoma cell motility. *Am J Pathol* **178,** 325-335 (2011).